Arabian Journal of Chemistry (2014) xxx, xxx–xxx

King Saud University

Arabian Journal of Chemistry

www.ksu.edu.sa
www.sciencedirect.com

ORIGINAL ARTICLE

Chitosan–ammonium acetate–ethylene carbonate membrane for proton batteries

Siti Salwa Alias, Siew Mian Chee, Ahmad Azmin Mohamad *

School of Materials and Mineral Resources Engineering, Universiti Sains Malaysia, 14300 Nibong Tebal, Penang, Malaysia

Received 30 May 2013; accepted 3 May 2014

KEYWORDS

Proton-conducting membrane;
Chitosan;
Cathode;
V_2O_5;
MnO_2;
Proton batteries

Abstract Proton-conducting membranes were prepared using a solution-casting technique. The highest membrane conductivity of $(3.83 \pm 0.73) \times 10^{-3}$ S cm^{-1} was achieved in chitosan acetate–50 wt.% ammonium acetate–70 wt.% ethylene carbonate. The batteries were fabricated with a configuration of Zn + $ZnSO_4 \cdot 7H_2O$ || chitosan membrane || MnO_2 and Zn + $ZnSO_4 \cdot 7H_2O$ || chitosan membrane || V_2O_5. The cathode materials produced open circuit voltages of 1.60 and 1.27 V using manganese (IV) oxide (MnO_2) and vanadium (IV) oxide (V_2O_5), respectively. The discharge capacities of the batteries were 45.0 and 34.7 mA h using MnO_2 and V_2O_5 cathode at 1.0 mA, respectively. The maximum power densities were 1.83 mW cm^{-2} for the battery with MnO_2 and 1.36 mW cm^{-2} for the battery with V_2O_5 cathode.

1. Introduction

The development of a low-cost proton-conducting membrane for proton battery has elicited considerable attention as an alternative to lithium (Li^+) ion battery (Ng and Mohamad, 2008). Besides the small size of the ionic radii proton (H^+)-conducting membrane that could be intercalated into the layered materials, this membrane also has the potential to deliver good electrochemical properties and economical materials. The lower proton electrochemical window (~1.0 V) provides greater improvement based on energy density compared with previous Li^+ ion batteries (~4.0 V) for small devices (Pratap et al., 2006).

Chitosan is one of the natural polymers that has a high degree of *N*-deacetylated form of chitin. Chitin is a naturally abundant mucopolysaccharide that serves as the supporting material of crustaceans, insects, and others (Dutta et al., 2004; Pillai et al., 2009). Chitosan has been applied as a proton-conducting membrane because of its excellent properties (Kadir et al., 2010; Ng and Mohamad, 2008). These properties include the following: (i) biocompatibility, biodegradable polymer, non-toxicity, and abundance in nature, (ii) existence of hydroxyl (OH^-) and amine (NH_3^+) functional groups, which have lone pair electrons at the chitosan monomer which allow the chelation of a proton (H^+) donor for battery, and (iii) chemically, thermally, and mechanically stable membrane (stable up to 200 °C) (Wan et al., 2006).

Normally, in proton-conducting polymer membranes, proton (H^+) species are contributed by the addition of salt. Ammonium acetate (NH_4CH_3COO) is one of the salts that has been doped in proton-conducting polymer membranes.

* Corresponding author. Tel.: +60 4599 6118; fax: +60 4594 1011.
E-mail address: aam@usm.my (A.A. Mohamad).

Peer review under responsibility of King Saud University.

Production and hosting by Elsevier

1878-5352
http://dx.doi.org/10.1016/j.arabjc.2014.05.001

Please cite this article in press as: Alias, S.S. et al., Chitosan–ammonium acetate–ethylene carbonate membrane for proton batteries. Arabian Journal of Chemistry (2014), http://dx.doi.org/10.1016/j.arabjc.2014.05.001

The conductivity of NH_4CH_3COO doped to polyvinyl alcohol resulted in a conductivity of approximately 10^{-6} S cm^{-1} (Hirankumar et al., 2005). Du et al. (2011, 2010) achieved a much higher conductivity of 10^{-4} S cm^{-1} when chitosan acetate (CA) membrane was complexed with 40 wt.% of NH_4CH_3COO. However, all the conductivity values obtained from the previous studies were still low ($\sim 10^{-5}$ S cm^{-1}) for the battery fabrication. Ethylene carbonate (EC) plasticizer has been doped to the CA membrane to increase the conductivity up to 10^{-3} S cm^{-1} (Kadir et al., 2010; Ng and Mohamad, 2006).

Several cathode material compositions have been reported in the literature, such as manganese (IV) oxide (MnO_2) (Ng and Mohamad, 2008; Dose and Donne, 2014), lead oxide (PbO_2) (Pratap et al., 2006; Chen et al., 2013), vanadium (III) oxide (V_2O_3) (Ali et al., 1998) and vanadium (IV) oxide (V_2O_5) (Pratap et al., 2006). The low operating voltage of V_2O_5 ($\sim$1.5 V) (Fergus, 2010; Feng et al., 2008) can still be used as cathode for proton batteries by adding high-surface area forms of carbon such as acetylene black to improve the contact between the cathode and the electrolyte (Fey et al., 2010; Jin et al., 2008; Ng and Mohamad, 2008).

Thus, this study aimed to investigate the influence of EC plasticizer amount on CA–NH_4CH_3COO membrane. The second goal was to fabricate the highest conductivity of CA–NH_4CH_3COO–EC membrane as Zn + $ZnSO_4{\cdot}7H_2O$ || CA–NH_4CH_3COO–EC || MnO_2 and Zn + $ZnSO_4{\cdot}7H_2O$ || CA–NH_4CH_3COO–EC || V_2O_5 proton batteries. This study also determined the electrochemical properties of the membrane, such as open circuit voltage (OCV), discharge characteristic, current–voltage (*I–V*), and current density–power density (*J–P*).

2. Experiment

2.1. Preparation and characterization of chitosan–NH_4CH_3COO–EC membranes

The membranes were prepared using the solution-casting technique. One gram chitosan powder (CP; Chito-Chem, Malaysia) was dissolved in 100 ml of 1% acetic acid solution (CH_3COOH, Wako Pure Chemical Industries). The mixture was continuously stirred with a magnetic stirrer at room temperature (25 °C). NH_4CH_3COO (RDH) and EC (Aldrich) were added accordingly at different concentrations. Once completely dissolved for 24 h, the solution was placed onto a Petri dish and left to dry at 25 °C to obtain membranes of CA, CA–NH_4CH_3COO, and CA–NH_4CH_3COO–EC systems as coded in Table 1. The membranes were maintained in desiccators with silica gel desiccants for further drying. The membranes were cut into suitable sizes and mounted on the conductivity holder with stainless steel (SS) electrodes under spring pressure. The conductivity of the dry membranes was determined using the Frequency Response Analyzer of Autolab PGSTAT 30 (Eco Chemie B.V.) in a frequency range between 1 Hz and 1 MHz. The measurements were carried out at 25 °C.

To determine the chemical functional group of the CA, CA–NH_4CH_3COO, and CA–NH_4CH_3COO–EC membrane systems, Fourier transform infrared (FTIR, Perkin–Elmer®) analysis was performed for all samples between 4000 and 550 cm^{-1} wave number. The membranes were selected based on the conductivity results.

Table 1 Amount of NH_4CH_3COO and EC in CA membranes.

Sample name	Chitosan (g)	NH_4 CH_3COO concentration (wt.%)	EC concentration (wt.%)
CP	1.0	–	–
CA	1.0	–	–
CA10N	1.0	10	–
CA20N	1.0	20	–
CA30N	1.0	30	–
CA40N	1.0	40	–
CA50N	1.0	50	–
CA60N	1.0	60	–
CA70N	1.0	70	–
CA50N10E	1.0	50	10
CA50N20E	1.0	50	20
CA50N30E	1.0	50	30
CA50N40E	1.0	50	40
CA50N50E	1.0	50	50
CA50N60E	1.0	50	60
CA50N70E	1.0	50	70

The mechanical properties of the selected CA, CA–NH_4CH_3COO, and CA–NH_4CH_3COO–EC membrane systems based on conductivity results were measured using a universal testing machine (Lloyd Instrument, 9911) at room temperature. All samples were cut into rectangular membranes (1.5 cm × 3 cm) before testing. A strain rate of 25 mm min^{-1} and gauge length of 50 mm were applied to the membranes.

2.2. Fabrication and characterization of proton batteries

The batteries were fabricated using the membrane with the highest conductivity. Zn powder (4.50 g; Merck) and $ZnSO_4{\cdot}7H_2O$ powder (1.50 g; Univar) were mixed with 0.15 g acetylene black (AB, Gunbai) and 0.05 g polytetrafluoroethylene (PTFE, Fluka) to form an anode pellet. Two different cathodes, namely, V_2O_5 (RDH) and MnO_2 (Aldrich) (4.50 g), were prepared by mixing with 0.40 g AB and 0.05 g PTFE to form cathode pellets. The current collector, SS mesh, was placed in the middle of both pellets. The batteries were designed as Zn + $ZnSO_4{\cdot}7H_2O$ || chitosan membrane || MnO_2 and Zn + $ZnSO_4{\cdot}7H_2O$ || chitosan membrane || V_2O_5 proton batteries.

The Arbin BT 2000 system was used to characterize the battery properties. The OCV of the batteries was measured for 48 h. The batteries were discharged using a constant current of 1.0 mA. The *I–V* and *J–P* curves were plotted using a discharge current ranging from 20 μA to 100 mA. The average voltage of both batteries was monitored for each current drain after a 10 s operation. All of the battery characteristics were measured using the galvanostat of Autolab PGSTAT 30 GPES (Eco Chemie B.V.).

3. Results and discussion

3.1. Conductivity of chitosan–NH_4CH_3COO–EC membranes

Fig. 1 depicts the variation of ionic conductivity of CA membrane as a function of NH_4CH_3COO and EC plasticizer contents at room temperature. The conductivity of CA increased proportionally with NH_4CH_3COO amounts (Fig. 1a). The

Please cite this article in press as: Alias, S.S. et al., Chitosan–ammonium acetate–ethylene carbonate membrane for proton batteries. Arabian Journal of Chemistry (2014), http://dx.doi.org/10.1016/j.arabjc.2014.05.001

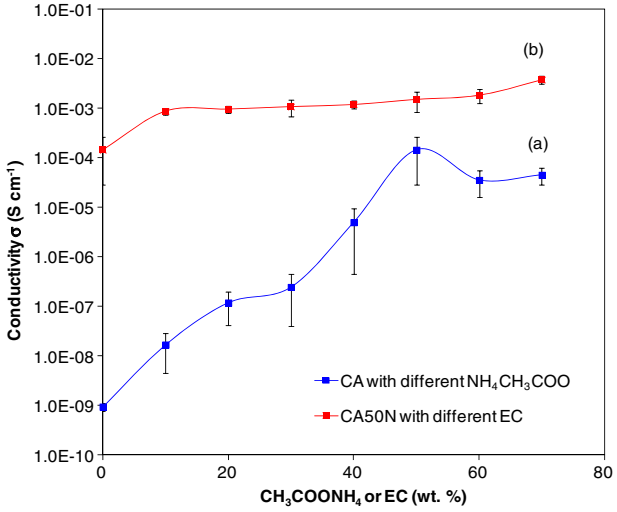

Figure 1 Conductivity of (a) CA with different concentrations of NH_4CH_3COO and (b) CA50N with different concentrations of EC.

CA conductivity in different NH_4CH_3COO amounts was between 10^{-10} and 10^{-4} S cm^{-1}. The highest conductivity of $(1.47 \pm 1.17) \times 10^{-4}$ S cm^{-1} was obtained by CA with 50 wt.% of NH_4CH_3COO (CA50N). However, when the amounts of NH_4CH_3COO increased to 60–70 wt.%, the conductivity steadily decreased.

Given that CA50N membrane had the highest conductivity value for CA–salt system, EC was added as a plasticizer to enhance its conductivity. Fig. 1b shows that the same trend also occurred in CA50N in different EC plasticizer contents. The conductivity progressively increased proportionally with EC contents. In addition, the conductivity was much higher compared with the CA–salt system at a range between 10^{-4} and 10^{-3} S cm^{-1} until 70 wt.% of EC. The highest conductivity of $(3.83 \pm 0.72) \times 10^{-3}$ S cm^{-1} was achieved in the CA50N70E membrane.

The sharp initial increase continued by gradually increasing the conductivity of CA in various NH_4CH_3COO concentrations. This phenomenon was attributed to the increase of free charge carrier movement in the membranes. When the optimum conductivity was reached, it started to decrease beyond the addition of 60–70 wt.% of NH_4CH_3COO. During the increase in conductivity, the charge carriers became more densely packed as the salt concentrations increased. Thus, the attractive interactions between these free charge carriers also increased (Lewandowski et al., 2001). However, when the conductivity decreased, the host matrix became more packed with dopant ions. This overcrowding reduced the number of charge carriers because of the limitation of charge carrier mobility (Ng and Mohamad, 2006).

The steady conductivity increase for CA50 as a function of EC plasticizer can be related to the negative dissociation of salt. In this case, EC did not increase the charge carrier numbers similar to its effect on the function of salt. However, EC assisted the dissociation of salt by increasing the number of mobile charge carriers. This increase in numbers led to conductivity enhancement compared to the unplasticized membrane (Ng and Mohamad, 2006).

3.2. Mechanical properties

Fig. 2 shows the tensile strength of CA, CA50N, CA70N, and CA50N70E membranes. Based on the results, the mechanical properties of SPEs were expected to decrease beyond 70 wt.% of EC because of the changing crystalline structure arrangement of the samples. The growth of larger crystals occurred beyond 70 wt.% of EC by expanding the smaller crystals. This growth will affect the tensile properties of the membrane. Low mechanical properties were not appropriate in applications for proton battery membranes. Table 2 presents the tensile values of the membranes.

To ensure adequate mechanical properties, the amount of EC was maintained at 70 wt.%, which was similar to the study of Ng and Mohamad (2008). Moreover, the tensile strength values were almost similar to the hydrated non-porous polypyrrole/chitosan between ~0.07 and 0.53 M Pa (Wan et al., 2004). Wan et al. (2004) stated that chitosan is a great hydrophilic and semi-crystalline copolymer because it contains polar hydroxyl and amino groups. The hydrogen bonding of inter- and intra-molecules, which formerly appeared in dry state, will no longer exist in the hydrated state of chitosan. Thus, the tensile strength indeed reduced.

3.3. FTIR analysis of chitosan–NH_4CH_3COO–EC membranes

Fig. 3 presents the FTIR spectra of CP, CH_3COOH solution, and CA membrane at 4000–2500 cm^{-1} and at 2000–500 cm^{-1}.

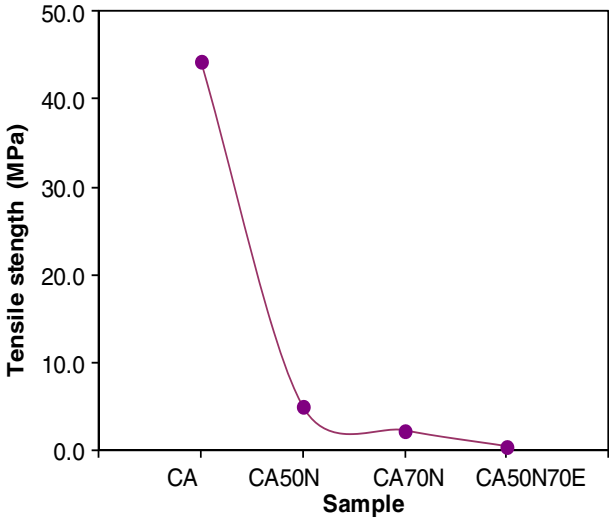

Figure 2 Tensile strength of CA, CA50N, CA70N, and CA50N70E.

Table 2 Tensile properties of membranes.

Sample	Tensile strength (M Pa)
CA	0.284
CA50N	0.032
CA70N	0.014
CA50N70E	0.003

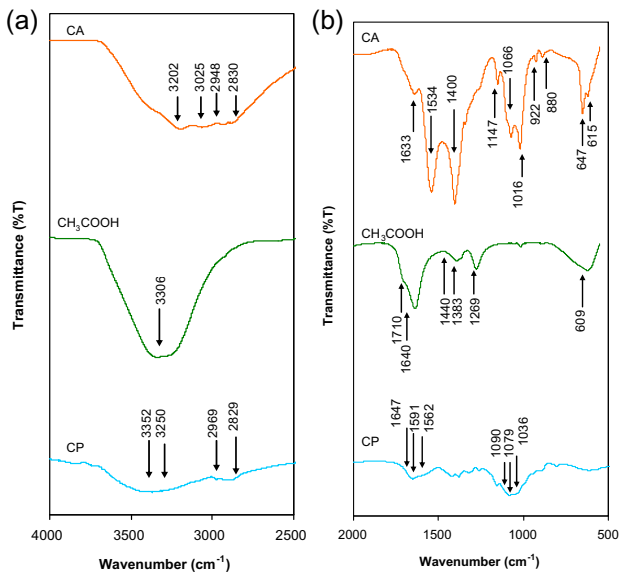

Figure 3 FTIR spectra for CP, CH_3COOH, and CA at (a) 4000–2500 cm^{-1} and at (b) 2000–500 cm^{-1}.

Some of the peaks shifted after the CP was dissolved in CH_3COOH solution. The new peaks of 3202 and 3025 cm^{-1} (CA membrane) were observed because of the shifting of 3352 cm^{-1} of CP (Tan et al., 2005) and 3306 cm^{-1} of CH_3COOH solution (stretching vibration of N–H and O–H bands). These peaks could be assigned to the axial stretching vibration of O–H superposed to the N–H stretching band and chitosan inter-hydrogen bonds (Enescu et al., 2009). The C–H band of CP at 2969 and 2829 cm^{-1} also stretched to 2948 and 2830 cm^{-1} (Fig. 3a).

In Fig. 3b, the symmetry of C═O stretch peak shifted from 1640 cm^{-1} (CH_3COOH solution) to 1633 cm^{-1} (CA membrane). In this study, the cation of CH_3COOH solution interacted with the nitrogen atom of NH_2 in chitosan. Consequently, NH_2 and other bands shifted. The existence of 1534 cm^{-1} confirmed the NH_2 deformation when peaks 1591 and 1562 cm^{-1} of CP shifted after dissolving in CH_3COOH solution (Yahya and Arof, 2003). The O–H band of CH_3COOH solution at 1440 cm^{-1} also shifted to 1400 cm^{-1} in CA membrane. Moreover, the C–O stretch of CH_3COOH solution shifted from 1383 and 1269 cm^{-1} to 1147 cm^{-1} of CA.

In addition, the C–O bond stretching vibration of CP at 1079 and 1036 cm^{-1} (Tan et al., 2005) shifted to 1066 and 1016 cm^{-1} in the CA membrane. The two new peaks exhibited were 992 and 880 cm^{-1} (C–O–H deformation). Meanwhile, the 647 and 615 cm^{-1} peaks of the CA membrane were denoted as a O–C═O bond shift of CH_3COOH solution (609 cm^{-1}). The shifting of some FTIR peaks proved that the CP dissolved well in CH_3COOH solution.

Fig. 4 shows the effects of various NH_4CH_3COO salt concentrations based on the FTIR spectra. The broad 3184 cm^{-1} peak (Fig. 4a) showed the NH_4^+ band, whereas the two broad bands of 2934 and 2820 represent the shift of the C–H stretch of chitosan acetate after the addition of NH_4CH_3COO (Fig. 4b). Moreover, the 1399 cm^{-1} peak (Fig. 4c) was referred to the NH_2 deformation of NH_4^+. This result proved that complexation occurred between the salt and the nitrogen atom of the amine group (Yahya and Arof, 2003). Other peaks exhibited in Fig. 4d and e were almost similar (overlaps) to those in Fig. 3a and b. However, the difference between CA, CA50N, and CA70N can still be observed based on the peak intensity.

All of the FTIR peaks of CA50N were higher compared with the CA and CA70N peaks. This result was attributed to the existence of the highest amount of charge carrier compared with the CA (without salt). Therefore, CA can easily complex with 50 wt.% of NH_4CH_3COO salt. On the other hand, CA70N had lower intensity of peaks compared with CA50N. The charge carrier of 70 wt.% of NH_4CH_3COO in CA70N reached the maximum dissociation to free charge carriers, and then associated again. The number of charge carrier that

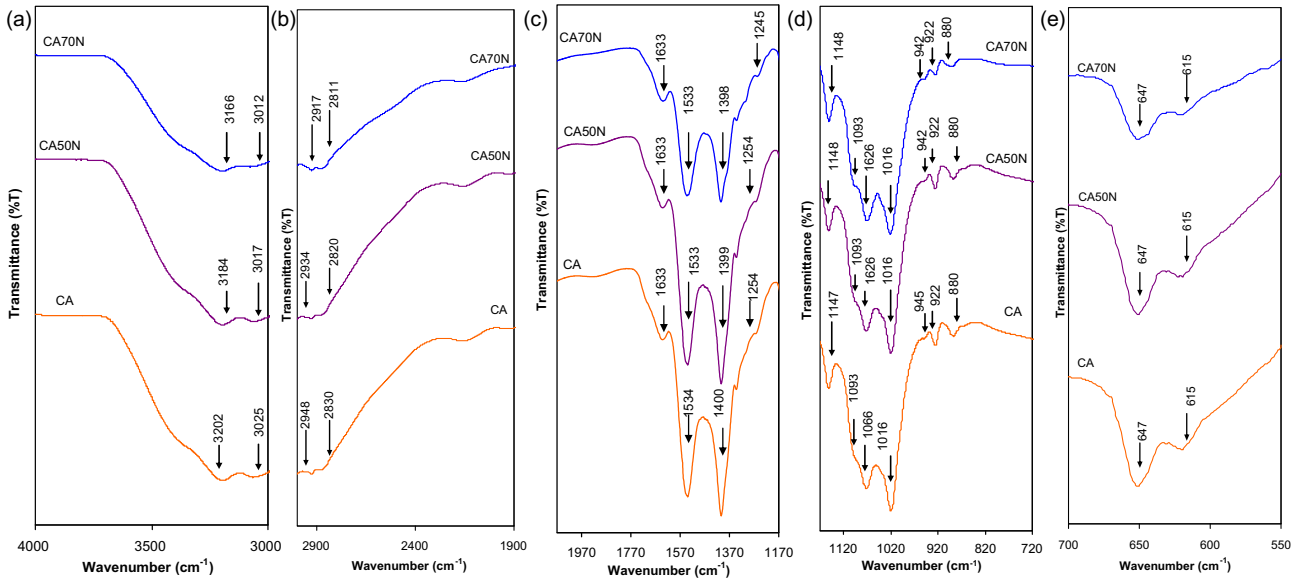

Figure 4 FTIR spectra for CA, CA50N, and CA70N at (a) 4000–3000 cm^{-1}, (b) 3000–2000 cm^{-1}, (c) 2070–1170 cm^{-1}, (d) 1170–720 cm^{-1}, and (e) 700–550 cm^{-1}.

can supply mobile protons reduced. Consequently, decreasing the complexation between the salt and the CA resulted in a decreased sample.

Fig. 5 depicts the effect of additional 70 wt.% EC to CA50N. This amount was selected for the analysis because it produced the highest membrane conductivity in this study. All the peaks of CA, CA50N, and CA50N70E existed as in Fig. 5a and b, which were almost similar to those in Figs. 3 and 4. The plasticizer (EC) only enhanced the interaction between the salt and the chitosan acid to form complexation. This enhancement implied that the plasticizer has the same function as the filler (Majid and Arof, 2009).

Nevertheless, six new peaks of EC were observed, as shown in Fig. 5c and d. These peaks were referred to as C═O stretch (1750 cm^{-1}) (Osman and Arof, 2003), C–C(O)–C stretch (1210 and 1160 cm^{-1}), symmetrical C–O–C stretch (1100 cm^{-1}), and O–C–O bond (764 and 709 cm^{-1}), which shifted to some new peaks for CA50N70E. Thus, this result demonstrated that complexation between CA50N and 70 wt.% of EC was good. Moreover, no significant peaks shifted in Fig. 5e. Table 3 summarizes all the functional groups in Figs. 3–5.

Fig. 6 illustrates the chemical interaction during the conduction mechanism between CP, CH_3COOH solution, CA, NH_4CH_3COO, and EC. The formation of hydrogen bond between CP and diluted CH_3COOH solution possibly occurred because chitosan contains a hydroxyl group (OH) along the chain (Fig. 6a). This formation was due to the existence of H—O–H in diluted CH_3COOH solution that can allow the formation of hydrogen bond, similar to the interaction between glycerol and water (Dashnau et al., 2006). In the same manner, hydrogen bonding occurred through the lone pair of the amine group, that is, $H_2N—H_2O$. The formation of hydrogen bond confirmed that CP can be dissolved in diluted CH_3COOH solution, which was supported by the FTIR analysis, thus contributing to the conduction mechanism.

Fig. 6b shows the interaction between the CA membrane and the NH_4CH_3COO at different concentrations. When different concentrations of NH_4CH_3COO were added to CA (in acidic media), the free amino group ($–NH_2$) of chitosan was protonated with H^+ ion of NH_4CH_3COO by hopping mechanism. Two of the four hydrogen atoms of NH_4^+ ions were identically bound. The third H^+ was bound more rigidly, whereas the fourth H^+ was bound more weakly. The weakly bound H^+ of NH_4^+ can easily be dissociated under the influence of an electric field. The movement of H^+ charge transportation in the bulk between the CA and the NH_4CH_3COO was similar to the previous study of ion movement in PEO electrolyte (Maurya et al., 1992). Nonetheless, beyond the addition of 60–70 wt.% of NH_4CH_3COO, the re-association of H^+ charge carriers (ion pairing) occurred when the salt reached its maximum dissociation to free H^+ charge carriers.

Fig. 6c shows the interaction between the CA50N membrane and the 70 wt.% EC. EC only moved along the CA50N70E chain because the EC plasticizer only contributed to the dissociation of salt enhancement and did not increase the H^+ charge carrier numbers. All of the conduction mechanisms were also supported by FTIR analysis in terms of chemical interactions between CP, CH_3COOH solution, NH_4CH_3COO, and EC plasticizer.

3.4. Surface morphology and structural properties of chitosan–NH_4CH_3COO–EC membrane

Fig. 7 shows the FESEM images and XRD diffractogram patterns of CP, CA, CA50N, CA70N, and CA50N70E membranes. Fig. 7a shows the scattered and bulky CP surface. The CP was partially crystalline, with a broad peak of 2θ between 16° and 24°. Upon mixing the CH_3COOH solution, the CA membrane surface became clear and uniform in appearance (Fig. 7b). The broad XRD peak of CA became less intense with the existence of some new peaks of 2θ between 12° and 40°. Meanwhile, the uniform morphology with a few small particles appeared when 50 wt.% of NH_4CH_3COO was added

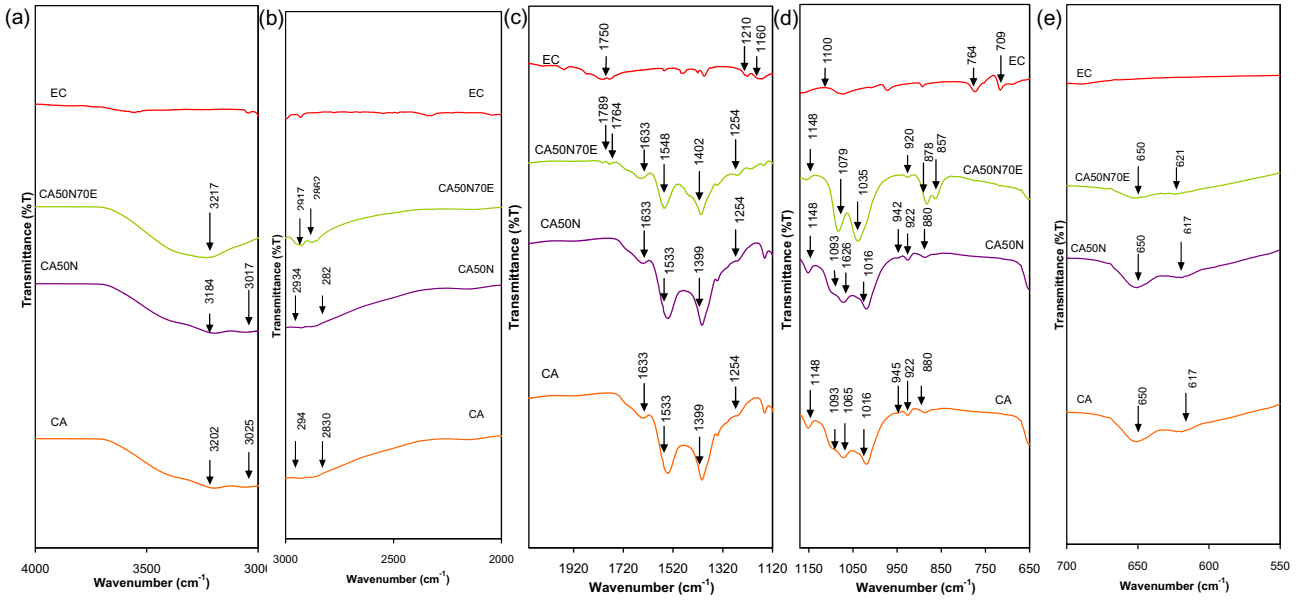

Figure 5 FTIR spectra for CA, CA50N, EC, and CA50N70E at (a) 4000–3000 cm^{-1}, (b) 3000–2000 cm^{-1}, (c) 2100–1120 cm^{-1}, (d) 1170–650 cm^{-1}, and (e) 700–550 cm^{-1}.

Table 3 FTIR of Chitosan–NH_4CH_3COO–EC membranes.

Sample name	Wave number (cm^{-1})	Functional group
Chitosan powder (CP)	3352	Stretching vibration of N–H and O–H
	3250	O–H band
	2969	C–H stretch
	2829	C–H stretch
	1647	NH_2 deformation
	1591	NH_2 deformation
	1562	NH_2 deformation
	1090	C–N stretch
	1079	Stretching vibration of C–O bond
	1036	Stretching vibration of C–O bond
Acetic acid (CH_3COOH)	3306	O–H stretch
	1710	C═O stretch
	1640	Symmetrical C═O stretch of dimmer
	1440	O–H bend
	1383	C–O stretch
	1269	C–O stretch
	609	O–C═O bend
CA	3202	Shifted of N–H band and O–H stretch
	3025	Shifted of O–H band and C–H stretch
	2948	Shifted of C–H stretch of chitosan
	2830	Shifted C–H stretch of chitosan
	1633	Shifted symmetrical C═O stretch of dimmer
	1534	Shifted of NH_2 deformation
	1400	Shifted O–H bend
	1147	Shifted C–O stretch of acetic acid
	1066	Shifted stretching vibration of C–O bond
	1016	Shifted stretching vibration of C–O bond
	992	C–O–H deformation
	880	C–O–H deformation
	647	Shifted of O–C═O bend
	615	Shifted of O–C═O bend
CA50N	3184	Shifted of N–H band and O–H stretch Broad band of NH_4^+
	3017	Shifted of O–H band and C–H stretch
	2934	Shifted of C–H stretch of chitosan-acetate
	2820	Shifted C–H stretch of chitosan-acetate
	1633	Shifted symmetrical C═O stretch of dimmer
	1533	Shifted of NH_2 deformation
	1399	NH_2 deformation of NH_4^+ ion
	1254	C–O stretch
	1148	Shifted C–O stretch of acetic acid
	1093	Shifted C–N stretch of acetic acid
	1065	Shifted C–N stretch acetic acid
	1016	Shifted stretching vibration of C–O bond from acetic acid
	945	Shifted of C–O–H deformation
	922	Shifted of C–O–H deformation
	880	Shifted of C–O–H deformation
	650	Shifted of O–C═O bend
	617	Shifted of O–C═O bend
CA70N	3166	Shifted of N–H band and O–H stretch Broad band of NH_4^+
	3012	Shifted of O–H band and C–H stretch
	2917	Shifted of C–H stretch of chitosan-acetate
	2811	Shifted C–H stretch of chitosan-acetate
	1633	Shifted symmetrical C═O stretch of dimmer
	1533	Shifted of NH_2 deformation
	1399	NH_2 deformation of NH_4^+ ion
	1254	C–O stretch
	1148	Shifted C–O stretch of acetic acid
	1093	Shifted C–N stretch of acetic acid
	1065	Shifted C–N stretch acetic acid

Please cite this article in press as: Alias, S.S. et al., Chitosan–ammonium acetate–ethylene carbonate membrane for proton batteries. Arabian Journal of Chemistry (2014), http://dx.doi.org/10.1016/j.arabjc.2014.05.001

Table 3 (*continued*)

Sample name	Wave number (cm^{-1})	Functional group
	1016	Shifted stretching vibration of C–O bond from acetic acid
	945	Shifted of C–O–H deformation
	922	Shifted of C–O–H deformation
	880	Shifted of C–O–H deformation
	650	Shifted of O–C═O bend
	617	Shifted of O–C═O bend
CA50N70E	3217	Shifted of N–H band and O–H stretch Broad band of NH_4^+
	2917	Shifted of C–H stretch of chitosan-acetate
	2862	Shifted C–H stretch of chitosan-acetate
	1789	Shifted C═O stretch after additional of EC
	1764	Shifted C═O stretch after additional of EC
	1633	Shifted symmetrical C═O stretch of dimmer
	1548	Shifted of NH_2 deformation
	1402	NH_2 deformation of NH_4^+ ion
	1254	C–O stretch
	1148	Shifted C–O stretch of acetic acid
	1079	Shifted symmetrical C–O–C stretch after additional of EC
	1035	Shifted symmetrical C–O–C stretch after additional of EC
	920	Shifted of C–O–H deformation
	878	Shifted of C–O–H deformation
	857	Shifted of C–O–H deformation
	650	Shifted of O–C–O bend after additional of EC Shifted of O–C═O bend
	621	Shifted of O–C–O bend after additional of EC Shifted of O–C═O bend
Ethylene carbonate (EC)	1750	C═O stretch
	1210	C–C(O)–C stretch
	1160	C–C(O)–C stretch
	1100	Symmetrical C–O–C stretch
	764	O–C–O bend
	709	O–C–O bend

to CA50N membrane, as shown in Fig. 7c. The three slightly broadened humps of XRD peaks appeared at $2\theta = 16°$, 30°, and 40°.

After the addition of 70 wt.% of NH_4CH_3COO, numerous small particles with rough surfaces can be observed on the CA70N membrane surface (Fig. 7d). Furthermore, the addition of NH_4CH_3COO resulted in a decreased intensity of three XRD humps in the CA70N membrane. Only the broad peak of 2θ that shifted between 16° and 40° can be observed because the peak of $2\theta = 30°$ diminished. However, in Fig. 7e, the CA50N70E membrane surface transformed into a slightly uniform surface, which was influenced by the EC plasticizer. The XRD broad peak was slightly increased and shifted to the left of $2\theta = 24°$.

The agglomerated and bulky surface was attributed to the partially crystalline CP, which agreed with the XRD results. Meanwhile, after mixing CH_3COOH solution with CP, the CA membrane surface turned clear and uniform because of the reaction between solid (CP) and liquid (CH_3COOH). The addition of 50 wt.% NH_4CH_3COO salt contributed to the smooth and uniform CA50N membrane surface. However, when the amount of NH_4CH_3COO reached 70 wt.%, the surface of the CA70N membrane became rough. This finding was attributed to the excess amount of salt reacting with CA solution. Compared with the CA70N membrane, the appearance of the CA50N70E membrane was jelly-like with a smooth surface. This surface was due to the plasticizer, which improved the structural properties of the membranes by steady enhancement in the polymer crystal and amorphous phase.

In general, the crystallinity of CP decreased upon mixing CH_3COOH solution with CA. Thus, the intensity of the broadened peak also decreased. When 50 wt.% NH_4CH_3COO was added to the samples, the original CP peaks ($2\theta = 20°$) shifted to the right ($2\theta = 30°$). This finding indicated that the crystallinity of the sample also further decreased and became an amorphous film. Meanwhile, further destruction of the CA70N membrane crystalline at $2\theta = 16$–40° was attributed to the reaction between the chitosan and the cation of salt (Majid and Arof, 2009). This destruction made the membrane too pliable, and thus, unsuitable for SPE application.

Nonetheless, in the CA50N70E membrane, the intensity of the broad peak slightly shifted to the left, implying the reaction between the chitosan membrane and the plasticizer. In this study, the plasticizer altered the membrane structure by moving along the membrane chain. The movement of this plasticizer directly opened and widened the path along the membrane chain and improved the structural properties. Thus, the CA50N70E membrane structure was better compared with the CA70N membrane surface. In addition, as shown in

Please cite this article in press as: Alias, S.S. et al., Chitosan–ammonium acetate–ethylene carbonate membrane for proton batteries. Arabian Journal of Chemistry (2014), http://dx.doi.org/10.1016/j.arabjc.2014.05.001

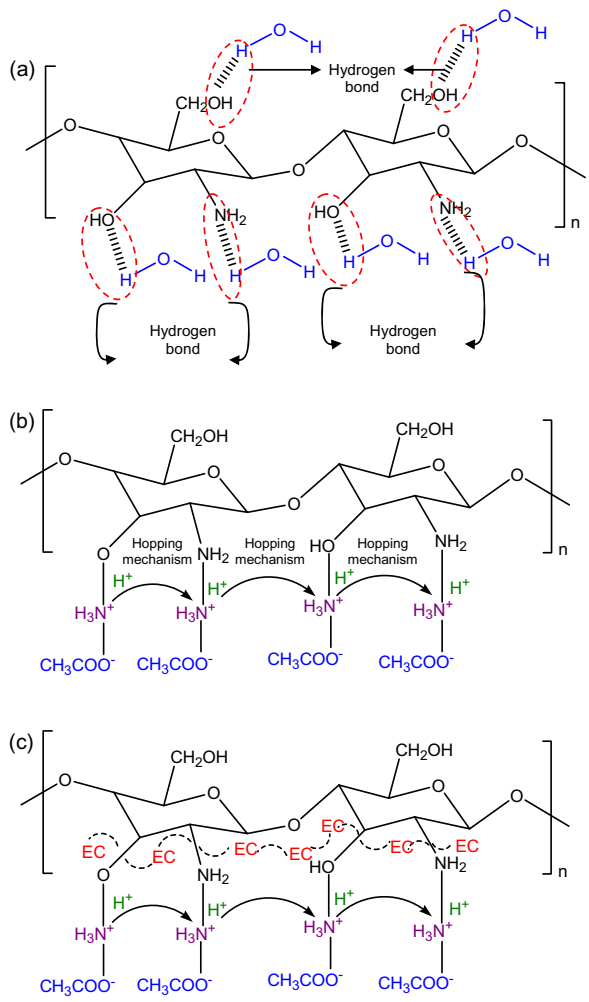

Figure 6 Interaction of (a) chitosan power and diluted CH_3COOH solution, (b) CA–NH_4CH_3COO, and (c) CA50N-70 wt.% EC.

FESEM, the CA50N70E membrane surface transformed to a more uniform surface compared with the CA70N membrane surface.

The XRD patterns and FESEM also supported the result of the conductivity study. The change in polymer–salt conductivity with the addition of different concentrations of salt and plasticizer indicated the structural changes within the samples (Koh et al., 2012). Moreover, the transformation of the membrane surface was observed as a result of the addition of NH_4CH_3COO and EC plasticizer.

Fig. 8 presents the EDX analysis of CP, CA, CA50N, CA70N, and CA50N70E membranes, which supported the FESEM images. The increasing amount of nitrogen wt.% in CA50N was proportional to the salt concentrations in CA70N. Nevertheless, the decrease of nitrogen wt.% in CA50N70E proved that the electron donor atoms in the polymer interacted with the salt cation and EC plasticizer.

3.5. Proton battery performance analysis

Fig. 9 shows the OCV of Zn + $ZnSO_4{\cdot}7H_2O$ || CA50N70E || MnO_2 and Zn + $ZnSO_4{\cdot}7H_2O$ || CA50N70E || V_2O_5 proton batteries. The proton battery using MnO_2 cathode was much more stable (1.60 V) compared with the proton battery using V_2O_5 (1.27 V) for 48 h. The stable potential provided better function and more durable proton battery. The chemical reactions that possibly occurred in the proton battery using MnO_2 cathode are as follows (Weast, 1977):

At the negative (anode) electrode, Zn was oxidized with the release of two electrons, and $ZnSO_4{\cdot}7H_2O$ provided the H^+ ions:

$$Zn \rightarrow Zn^{2+} + 2e^- \quad E^\circ_{ox} = 0.76\ V \tag{1}$$

$$ZnSO_4 \cdot 7H_2O \rightarrow 7H^+ + 7OH^- + ZnSO_4 \quad E^\circ_{ox} = -0.82\ V \tag{2}$$

- At the positive (cathode) electrode, MnO_2 was reduced with the acceptance of electrons:

$$MnO_2 + 2e^- + 4H^+ \rightarrow Mn^{2+} + 2H_2O \quad E^\circ_{red} = 1.22\ V \tag{3}$$

- The overall proton battery reaction was calculated based on the standard electrode potential (the oxidation potential was the negative value of the reduction potential) (Linden, 2002):

$$E^\circ_{ox} + E^\circ_{red} = E^\circ_{cell}$$

$$Zn + ZnSO_4 \cdot 7H_2O + MnO_2 + 2e^- + 4H^+ \rightarrow Zn^{2+} + 7H^+ + 7OH^- + ZnSO_4 + Mn^{2+} + 2H_2O - (0.76 - 0.82)\ V + 1.22\ V = 1.28\ V \tag{4}$$

For the proton battery using V_2O_5 cathode, the reaction is as follows (Weast, 1977):

- At the negative (anode) electrode, Zn was oxidized with the release of two electrons, and $ZnSO_4{\cdot}7H_2O$ provided the H^+ ions:

$$Zn \rightarrow Zn^{2+} + 2e^- \quad E^\circ_{ox} = 0.76\ V \tag{5}$$

$$ZnSO_4 \cdot 7H_2O \rightarrow 7H^+ + 7OH^- + ZnSO^4 \quad E^\circ_{ox} = -0.82\ V \tag{6}$$

- At the positive (cathode) electrode, V_2O_5 was reduced with the acceptance of electrons:

$$V_2O_5 + 2e^- + 6H^+ \rightarrow 2VO^{2+} + 3H_2O \quad E^\circ_{red} = 0.96\ V \tag{7}$$

- The overall proton battery reaction is as follows:

$$E^\circ_{ox} + E^\circ_{red} = E^\circ_{cell}$$

$$Zn + ZnSO_4 \cdot 7H_2O + V_2O_5 + 2e^- + 6H^+ \rightarrow Zn^{2+} + 7H^+ + 7OH^- + ZnSO_4 + 2VO^{2+} + 3H_2O - (0.76 - 0.82)\ V + 0.96\ V = 1.02\ V \tag{8}$$

In this study, the overall reaction provided the cell with E°_{cell} of 1.28 and 1.02 V for proton battery using MnO_2 and V_2O_5. However, the E°_{cells} of both batteries were 1.60 and 1.27 V, respectively. Eqns. (2)–(8) are possible because the fabrication of both batteries achieved OCV values higher than the theoretical calculation. The OCV values obtained in this study

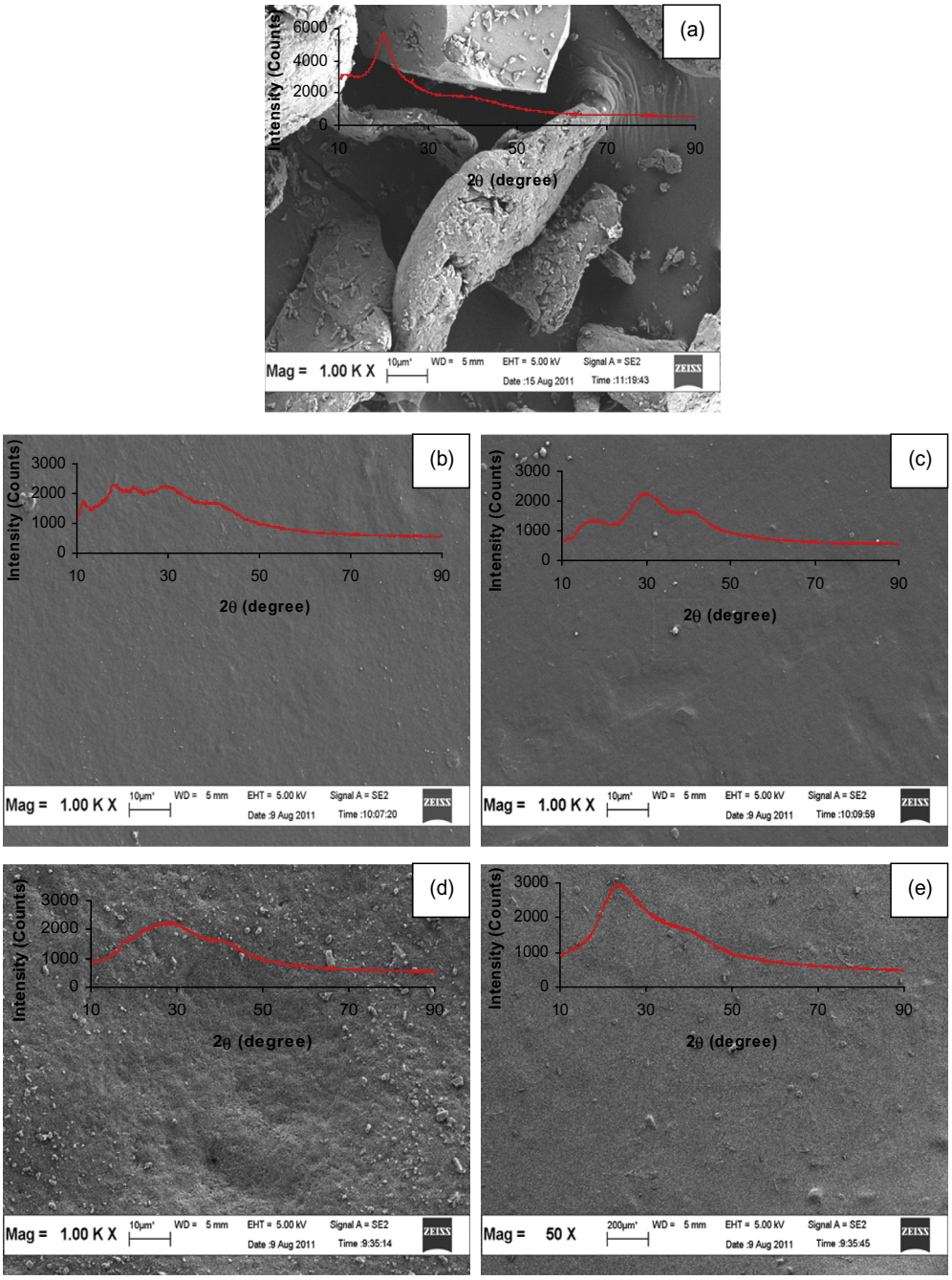

Figure 7 FESEM and XRD images of (a) chitosan powder, (b) CA, (c) CA50N, (d) CA70N, and (e) CA50N70E.

were more or less the same with the values obtained by previous works on proton battery using the same cathode materials (MnO_2 and V_2O_5), which were 1.56 (Ng and Mohamad, 2006), 1.57 (Pratap et al., 2006), and 1.48 V (Ng and Mohamad, 2008).

Fig. 10 indicates the discharge profile of Zn + $ZnSO_4 \cdot 7H_2O$ || CA50N70E || MnO_2 and Zn + $ZnSO_4 \cdot 7H_2O$ || CA50N70E || V_2O_5 proton batteries at 1.0 mA. The initial voltages of the proton batteries that used MnO_2 and V_2O_5 cathodes were 1.59 and 1.39 V, respectively. The results showed that both voltages were reduced to 0.50 V after sustaining for 52 min (MnO_2) and 49 min (V_2O_5). The discharge capacities of the proton batteries using MnO_2 and V_2O_5 cathode were 45.0 and 34.7 mA h, respectively. Based on the discharge profile, the proton batteries using MnO_2 cathode achieved higher discharge capacity compared with those using V_2O_5 cathode. In general, cathode materials are reactive with well-known electrolyte solutions, thus achieving rich surface chemistry (Aurbach et al., 2007).

The maximum discharge current was controlled by the three processes that occurred during discharge: (i) hydrogen was inserted into the cathode material, (ii) electrons from the anode reduced Mn^{2+} and VO^{2+} ions in the cathode to a lower valence, and (iii) admittance of the H^+ ions in the electrolyte to the electrode surface. Exchange of H^+ ions with the electrolyte occurred at the electrode–electrolyte interface. Besides the

intrinsic electrochemical properties of the material, cathode performance depended significantly on the electrode microstructure and morphology. These reactions were almost similar to the cathode materials for Li^+ batteries (Fergus, 2010).

The discharge capacity of the battery with V_2O_5 cathode was lower compared with the battery with MnO_2 cathode. This finding was attributed to the properties of V_2O_5. Generally, V_2O_5 has a high specific capacity of crystallinity. However, V_2O_5 undergoes structural conversion produced by the mechanical stress during deep charge–discharge cycles. Therefore, this conversion directly reduces the battery specific capacity besides decreasing the operating voltages (Fergus, 2010; Feng et al., 2008).

Fig. 11 shows the characteristics of *I–V* and *J–P* of $Zn + ZnSO_4{\cdot}7H_2O \parallel CA50N70E \parallel MnO_2$ and $Zn + ZnSO_4{\cdot}7H_2O \parallel CA50N70E \parallel V_2O_5$ proton batteries using current drains ranging from 2 μA to 100 mA. The voltage dropped from 1.70 to 0.34 V for the proton battery using MnO_2. Meanwhile, for the proton battery with V_2O_5, the voltage dropped from 1.56 V to 0.40 V. The maximum power densities were 1.83 mW cm^{-2} for the battery with MnO_2 and 1.36 mW cm^{-2} for the battery with V_2O_5 cathode based on the *J–P* curves.

The *I–V* curves for both batteries were linear, which denoted that the ohmic contribution was mainly controlled for the polarization of the electrode. However, the maximum power densities obtained for both batteries were lower compared with those from prior studies (Kadir et al., 2010; Ng and Mohamad, 2006, 2008). These lower densities were attributed to the adhesion between the electrolyte and the MnO_2 surface, which was contributed by the battery properties. On the other hand, in the study done by Pratap et al., (2006),

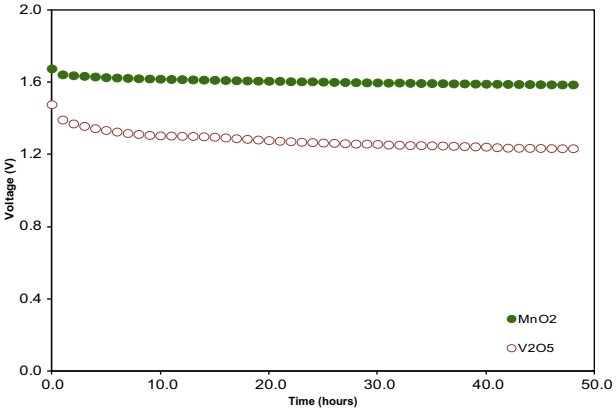

Figure 9 Open circuit voltage of proton batteries using CA50N70E membranes.

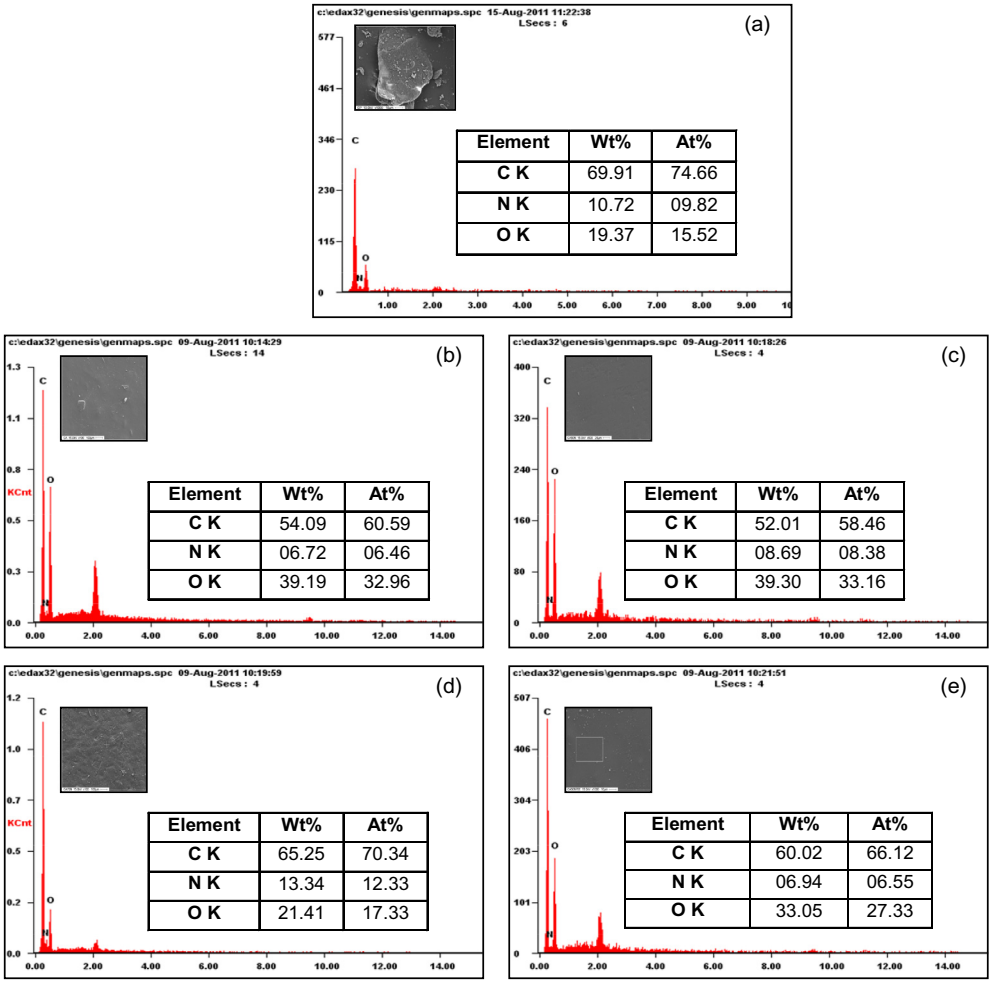

Figure 8 EDX of (a) chitosan powder, (b) CA, (c) CA50N, (d) CA70N, and (e) CA50N70E.

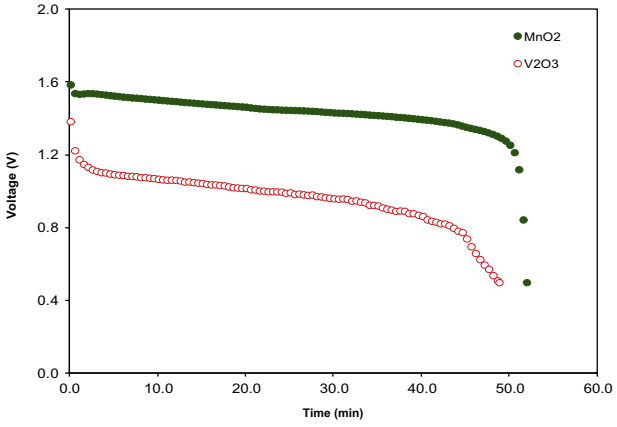

Figure 10 Discharge profile at 1.0 mA of proton batteries using CA50N70E membranes.

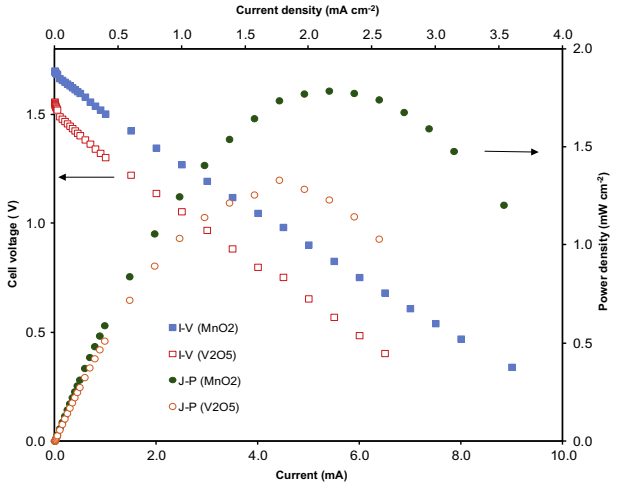

Figure 11 Plot of *I–V* and *J–P* using CA50N70E membranes for proton batteries.

V_2O_5 has been mixed with other intercalating oxides such as PbO_2 in order to give a better battery performance.

4. Conclusion

This study obtained the highest conductivity of $(3.83 \pm 0.73) \times 10^{-3}$ S cm^{-1} in the CA50N70E membrane. This membrane also had optimum morphological and structural properties. The battery with configuration of Zn + $ZnSO_4 \cdot 7H_2O$ || CA50N70E || MnO_2 achieved the best electrochemical properties, with an OCV value of 1.60 V. The discharge capacity of this battery at 1.0 mA was 45.00 mA h, and the maximum power density was 1.83 mW cm^{-2}.

Acknowledgement

SSA would like to thank MyPhD scholarship. A.A.M. wishes to thank the ERGS (203/PBahan/6730006) for the financial support for this study.

References

Ali, A.M.M., Mohamed, N.S., Arof, A.K., 1998. Polyethylene oxide (PEO)–ammonium sulfate ($(NH_4)_2SO_4$) complexes and electrochemical cell performance. J. Power Sources 74, 135–141.

Aurbach, D., Markovsky, B., Salitra, G., Markevich, E., Talyossef, Y., Koltypin, M., Nazar, L., Ellis, B., Kovacheva, D., 2007. Review on electrode–electrolyte solution interactions, related to cathode materials for Li-ion batteries. J. Power Sources 165, 491–499.

Chen, T., Ma, H., Kong, D., 2013. Discharge performance of nanostructured PbO_2 microspheres as the positive active material. Mater. Lett. 90, 103–106.

Dashnau, J.L., Nucci, N.V., Sharp, K.A., Vanderkooi, J.M., 2006. Hydrogen bonding and the cryoprotective properties of glycerol/water mixtures. J. Phys. Chem. B 110, 13670–13677.

Dose, W.M., Donne, S.W., 2014. Optimising heat treatment environment and atmosphere of electrolytic manganese dioxide for primary Li/MnO_2 batteries. J. Power Sources 247, 852–857.

Du, J., Bai, Y., Chu, W., Qiao, L., 2011. The microstructure and performance of solid-state hydrogen sensor using CH_3COONH_4-doped chitosan as electrolyte. J. Appl. Electrochem. 41, 183–187.

Du, J.F., Bai, Y., Chu, W.Y., Qiao, L.J., 2010. The structure and electric characters of proton-conducting chitosan membranes with various ammonium salts as complexant. J. Polym. Sci., Part B: Polym. Phys. 48, 880–885.

Dutta, P.K., Dutta, J., Tripathi, V.S., 2004. Chitin and Chitosan: Chemistry, Properties and Applications. CSIR.

Enescu, D., Hamciuc, V., Ardeleanu, R., Cristea, M., Ioanid, A., Harabagiu, V., Simionescu, B.C., 2009. Polydimethylsiloxane modified chitosan. Part III: preparation and characterization of hybrid membranes. Carbohydr. Polym. 76, 268–278.

Feng, C.Q., Wang, S.Y., Zeng, R., Guo, Z.P., Konstantinov, K., Liu, H.K., 2008. Synthesis of spherical porous vanadium pentoxide and its electrochemical properties. J. Power Sources 184, 485–488.

Fergus, J.W., 2010. Recent developments in cathode materials for lithium ion batteries. J. Power Sources 195, 939–954.

Fey, G.T.-K., Chang, C.-S., Kumar, T.P., 2010. Synthesis and surface treatment of $LiNi_{1/3}Co_{1/3}Mn_{1/3}O_2$ cathode materials for Li-ion batteries. J. Solid State Electrochem. 14, 17–26.

Hirankumar, G., Selvasekarapandian, S., Kuwata, N., Kawamura, J., Hattori, T., 2005. Thermal, electrical and optical studies on the poly(vinyl alcohol) based polymer electrolytes. J. Power Sources 144, 262–267.

Jin, B., Gu, H.-B., Kim, K.-W., 2008. Effect of different conductive additives on charge/discharge properties of LiCoPO4/Li batteries. J. Solid State Electrochem. 12, 105–111.

Kadir, M.F.Z., Majid, S.R., Arof, A.K., 2010. Plasticized chitosan–PVA blend polymer electrolyte based proton battery. Electrochim. Acta 55, 1475–1482.

Koh, J.C., Ahmad, Z.A., Mohamad, A.A., 2012. Bacto agar-based gel polymer electrolyte. Ionics 18, 359–364.

Lewandowski, A., Zajder, M., Frąckowiak, E., Béguin, F., 2001. Supercapacitor based on activated carbon and polyethylene oxide–KOH–H2O polymer electrolyte. Electrochim. Acta 46, 2777–2780.

Linden, D., 2002. Basics concepts. In: Reddy, T.B. (Ed.), Handbook of Batteries. McGraw-Hill.

Majid, S.R., Arof, A.K., 2009. Conductivity studies and performance of chitosan based polymer electrolytes in H_2/air fuel cell. Polym. Adv. Technol. 20, 524–528.

Maurya, K.K., Srivastava, N., Hashmi, S.A., Chandra, S., 1992. Proton conducting polymer electrolyte: II polyethylene oxide + NH_4I system. J. Mater. Sci. 27, 6357–6364.

Ng, L.S., Mohamad, A.A., 2006. Protonic battery based on a plasticized chitosan-NH_4NO_3 solid polymer electrolyte. J. Power Sources 163, 382–385.

Ng, L.S., Mohamad, A.A., 2008. Effect of temperature on the performance of proton batteries based on chitosan–NH_4NO_3–EC membrane. J. Membr. Sci. 325, 653–657.

Osman, Z., Arof, A.K., 2003. FTIR studies of chitosan acetate based polymer electrolytes. Electrochim. Acta 48, 993–999.

Pillai, C.K.S., Paul, W., Sharma, C.P., 2009. Chitin and chitosan polymers: chemistry, solubility and fiber formation. Prog. Polym. Sci. 34, 641–678.

Pratap, R., Singh, B., Chandra, S., 2006. Polymeric rechargeable solid-state proton battery. J. Power Sources 161, 702–706.

Tan, X.-C., Tian, Y.-X., Cai, P.-X., Zou, X.-Y., 2005. Glucose biosensor based on glucose oxidase immobilized in sol–gel chitosan/silica hybrid composite film on Prussian blue modified glass carbon electrode. Anal. Bioanal. Chem. 381, 500–507.

Wan, Y., Creber, K.aq.M., Peppley, B., Tam Bui, V., 2006. Chitosan-based solid electrolyte composite membranes: I. Preparation and characterization. J. Membr. Sci. 280, 666–674.

Wan, Y., Wu, H., Wen, D., 2004. Porous-conductive chitosan scaffolds for tissue engineering, 1: Preparation and characterization. Macromol. Biosci. 4, 882–890.

Weast, R.C., 1977. CRC Handbook of Chemistry and Physics: A Ready-Reference Book of Chemical and Physical Data. CRC Press.

Yahya, M.Z.A., Arof, A.K., 2003. Effect of oleic acid plasticizer on chitosan–lithium acetate solid polymer electrolytes. Eur. Polymer J. 39, 897–902.

Please cite this article in press as: Alias, S.S. et al., Chitosan–ammonium acetate–ethylene carbonate membrane for proton batteries. Arabian Journal of Chemistry (2014), http://dx.doi.org/10.1016/j.arabjc.2014.05.001